VERSITA

Numerical Support of Laboratory Experiments: Attenuation and Velocity Estimations

Erik H. SAENGER, Claudio MADONNA, Marcel FREHNER, and Bjarne S.G. ALMQVIST

ETH Zurich Geological Institute, Zurich, Switzerland
e-mail: erik.saenger@erdw.ethz.ch

Abstract

We show that numerical support of laboratory experiments can significantly increase the understanding and simplify the interpretation of the obtained laboratory results. First we perform simulations of the Seismic Wave Attenuation Module to measure seismic attenuation of reservoir rocks. Our findings confirm the accuracy of this system. However, precision can be further improved by optimizing the sensor positions. Second, we model wave propagation for an ultrasonic pulse transmission experiment used to determine pressure- and temperature-dependent seismic velocities in the rock. Multiple waves are identified in our computer experiment, including bar waves. The metal jacket that houses the sample assembly needs to be taken into account for a proper estimation of the ultrasonic velocities. This influence is frequency-dependent.

Key words: numerical modelling, ultrasonic velocities, seismic attenuation.

1. INTRODUCTION

Only in rather simple cases the propagation of elastic waves can be described by exact analytical expressions. Numerical techniques have to be applied for complex geometries, which are usually present in laboratory experimental setups to measure attenuation and ultrasonic velocities. In this paper we consider the influence of the laboratory setup on the obtained results. We discuss two different experiments performed in the Rock Deforma-

tion Lab of the ETH Zurich. However, our findings can also be generalized and applied to similar experiments performed with other instrumental setups for seismic attenuation (O'Connell and Budiansky 1977, Spencer 1981, Batzle *et al.* 2006) and for ultrasonic velocity measurements (Christensen 1979, Jackson and Paterson 1987, Kern *et al.* 1999, Kono *et al.* 2004).

2. NUMERICAL MODELING

For solving the elastodynamic wave equation we use the rotated staggered grid finite-difference technique (Saenger *et al.* 2000). This method has already been applied at the microscale using digital rock images (Saenger *et al.* 2011), as well as at the field scale (Steiner and Saenger 2012). The viscoelastic extension is described in detail in Saenger *et al.* (2005).

3. SIMULATION OF ATTENUATION MEASUREMENTS (2D)

Seismic attenuation in extensional mode is measured employing the Seismic Wave Attenuation Module (SWAM; see Fig. 1). The module hosts cylindrical rocks samples. It is designed to operate under confining pressure and at a strain below 10^{-6}, where the rock can be assumed to behave linearly. Seismic frequencies are systematically scanned from 10^{-2} up to 10^{2} Hz and the pore pressure of the fluid-saturated sample can be controlled. The attenuation (Q_E) and the Young's modulus are obtained using the sub-resonance method (Lakes 2009). The rock sample is cyclically stressed and the phase shift, ϕ, between the stress and the strain signals is used to calculate Q_E according to the equation

$$Q_E^{-1} = \tan \phi \ .$$

The technical details of the SWAM are described in Madonna and Tisato (2013). Numerical simulations were carried out to understand the influence of the following parameters on the measurements of Q_E: (i) position of the displacement sensors (LVDTs), (ii) stiffness of the sample, (iii) confining medium, and (iv) interface types to induce different saturation modes.

For this purpose we created a 2D viscoelastic numerical model of the SWAM (Fig. 2). The numerical setup consists of a regular grid with 26×96 grid points. With up to 24 million time steps the viscoelastic simulations take up to 6 hours on a standard dual-core laptop.

The 2D model (grid spacing 0.25 cm) consists of a 6.5×24 cm area. The elastic parameters of the different materials are given in Table 1. A sinusoidal vertical displacement source ($f = [1 - 10000$ Hz]) is acting on the top, while the bottom is fixed. For each simulation the time increment was kept constant at $\Delta t = 3.8 \times 10^{-7}$ s, which is determined by the grid spacing and the maximum elastic modulus in the model. However, for the applied fre-
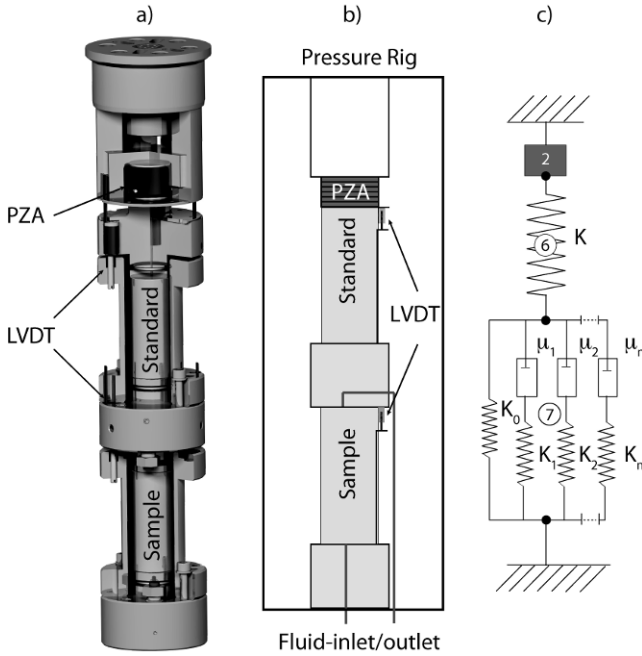
Fig. 1. Schematic cross-section of the ETH-developed SWAM: (a) CAD drawing, (b) sketched construction, and (c) physical model consisting of a piezo-electric actuator (PZA); an elastic reference sample (1), and the measured sample represented as a generalized Maxwell-body (2). Figure modified after Madonna and Tisato (2013).

Table 1

Material properties used for the SWAM simulations

Material	Bulk modulus K [GPa]	Shear modulus μ [GPa]	Density [kg/m^3]
Aluminum	114	25	2698
Steel	231.6	77.2	8000
Plexiglas	2.79	1.7	1185
Rock	69.7	23.2	2680
Vacuum	0	0	0.001

Note: The attenuation of the sample (*i.e.*, plexiglas and rock) is set for the applied excitation frequency to $Q = 12.33$ (Saenger *et al.* 2005).

quencies, this time increment is relatively small. The modeling is done with second order time update and with second order spatial differentiation operators.
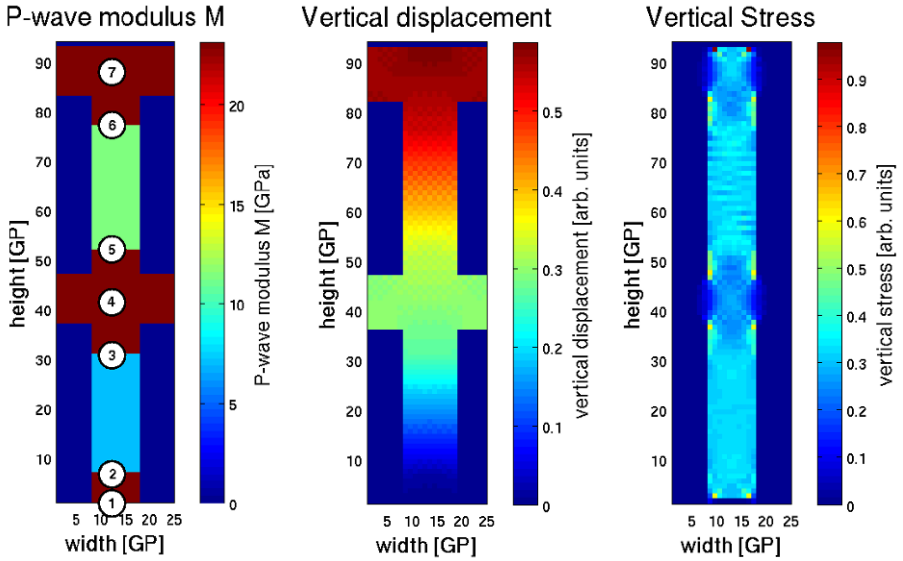
Fig. 2. Left-hand side: *P*-wave modulus, *M*, of the different parts of the 2D SWAM model. The aluminum reference sample is located between the sensor positions (SP) 5 and 6; the measured sample (rock or plexiglas) is located between SP 2 and 3. As a confining medium we used vacuum (dark blue region). Center: Vertical displacement during a simulation. Right-hand side: The vertical stress is relatively homogeneous in the aluminum, as well as in the rock sample. Axis scales are in grid points (GP). Colour version of this figure is available in electronic edition only.

The vertical displacements were recorded for two different configurations of the LVDTs. The positions of the sensors (SP) are reported in Fig. 2. The simulations were repeated for two different sample stiffnesses using either rock or plexiglas values.

The first configuration reflects the real position of the LVDTs, where the displacement of the elastic element is measured between the points SP7-SP4 and the displacement of the sample is measured between the points SP4-SP1 (Fig. 2). The result is plotted as $Q_{E\text{-real}}$ in Figs. 3 and 4.

The second configuration reflects the ideal position of the LVDTs, where the displacement of the elastic element is measured between the points SP6-SP5 and the displacement of the sample is measured between the points SP3-SP2 (Fig. 2). The result is plotted as $Q_{E\text{-opt}}$ in Figs. 3 and 4. The latter configuration considers only the displacement of the sample and the standards, whereas in the first case a small portion of the stainless steel is present, which in practice allows sealing the sample with a jacket.
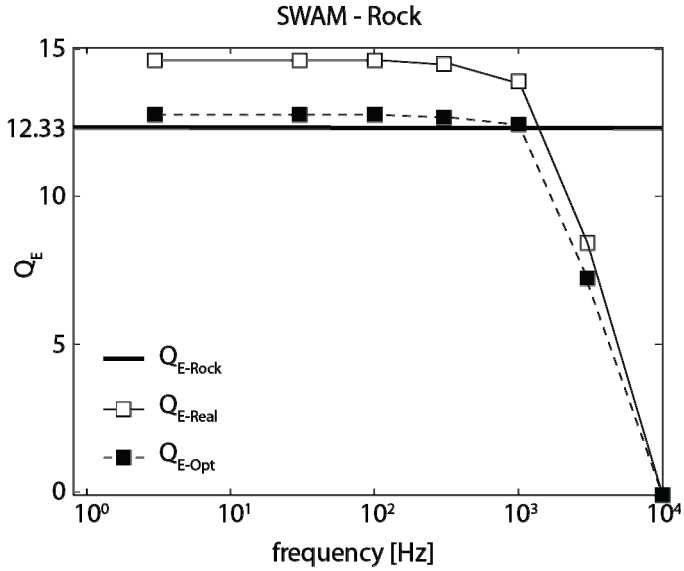
SWAM - Rock

Fig. 3. Results of the SWAM computer experiments for a plexiglas sample with an attenuation of $Q_E = 12.33$ (bold line) for a range of applied excitation frequencies. $Q_{E\text{-real}}$ (thin line) can be compared with the real experimental setup. An optimized sensor positioning allows for more accurate measurements of Q_E ($Q_{E\text{-opt}}$; dashed line).
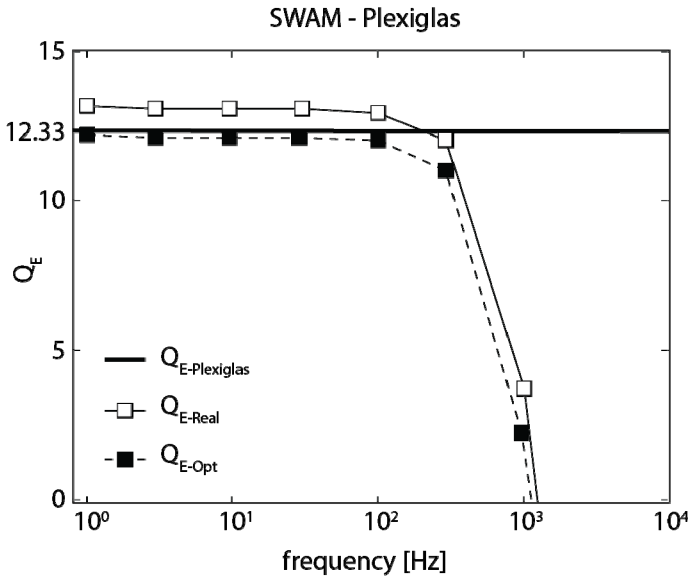
SWAM - Plexiglas

Fig. 4. SWAM computer experiments, as described in Fig. 3, but for the rock sample.

The main results of our computational experiments are given in Figs. 3 and 4 for plexiglas and rock, respectively. Below, we summarize our main findings:

  ❑ Q_E can be measured very accurately with the used experimental setup. However, for frequencies around or higher than 100 Hz the results are less accurate. They are disturbed by resonance effects of the module.

  ❑ The attenuation can be measured more accurately for samples of lower stiffness (comparison of $Q_{E\text{-real}}$-plexiglas *versus* $Q_{E\text{-real}}$-rock).

  ❑ The SWAM can be improved by repositioning the sensors. $Q_{E\text{-opt}}$ is more accurate than $Q_{E\text{-real}}$.

  ❑ Additionally, we tested other confining media (*e.g.*, oil) and interface heterogeneities to the sample. These factors do not influence the measurements significantly (not shown here).

4. SIMULATION OF VELOCITY MEASUREMENTS (3D)

Ultrasonic velocity measurements at elevated pressures and temperatures are routinely performed in the laboratory to investigate rock *P*- and *S*-wave velocities at pressure and temperature conditions representing *in situ* conditions of the Earth's crust and upper mantle (*e.g.*, Burlini *et al.* 2005, 2007, Ferri *et al.* 2007, Caricchi *et al.* 2008). For this purpose, the internally heated Paterson gas-medium apparatus (Fig. 5) is used at the ETH Zurich, with the possibility to reach pressures and temperatures of up to 500 MPa and 1200°C.

To simulate the ultrasonic experiments of the sample assembly we used a 3D model area with $1275 \times 118 \times 118$ grid points. A cubic elementary cell with an edge length of 1.5×10^{-4} m is chosen. The elastic moduli that were used are summarized in Table 2.

We used a body force in the vertical direction ($f = 0.1$ or 0.5 MHz) at the top transducer position (Fig. 5). The source function is the first derivative of a Gaussian with a time step of 1.125×10^{-8} s. The finite difference algorithm comprises a second order time update and second order space differentiation operators.

Table 2

Used material properties for the ultrasonic simulations

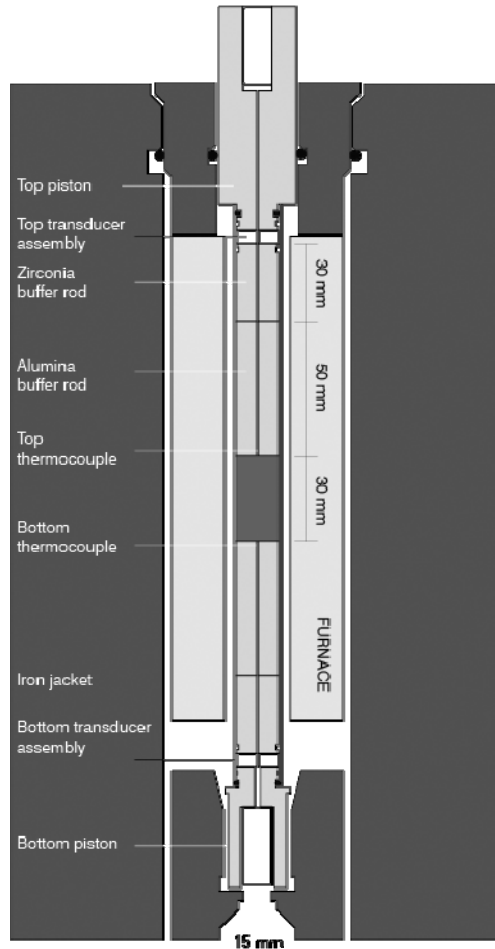| Material	Bulk modulus K [GPa]	Shear modulus μ [GPa]	Density [kg/m^3]
Alumina	228	152	3890
Zirconia	171	79	6130
Sapphire	307	147	3886
Rock	69.7	23.2	2680
Jacket	166.7	81.5	7874

Fig. 5. Sample assembly for ultrasonic velocity measurements in the Paterson gas-medium apparatus (redrawn from Burlini *et al.* 2005). The sample is buffered on each side by aluminum and zirconia rods, which act as thermal insulators protecting the piezoelectric crystals. The assembly is covered by an impermeable iron or copper jacket (thickness of 1 mm) that prevents the confining medium (argon gas) to enter the sample. The length from top to bottom transducer is 190 mm.

Figures 6 and 7 show the vertical displacement at the bottom receiver for an exitation frequency of 0.1 and 0.5 MHz, respectively. As expected, the velocity and amplitude of the waves strongly depend on the frequency of the simulated signal. Even though a relatively simple source-time function is introduced, the received signal looks rather complicated due to wave conversion and multiple reflections. It is not straightforward to pick the correct first-arrival times.

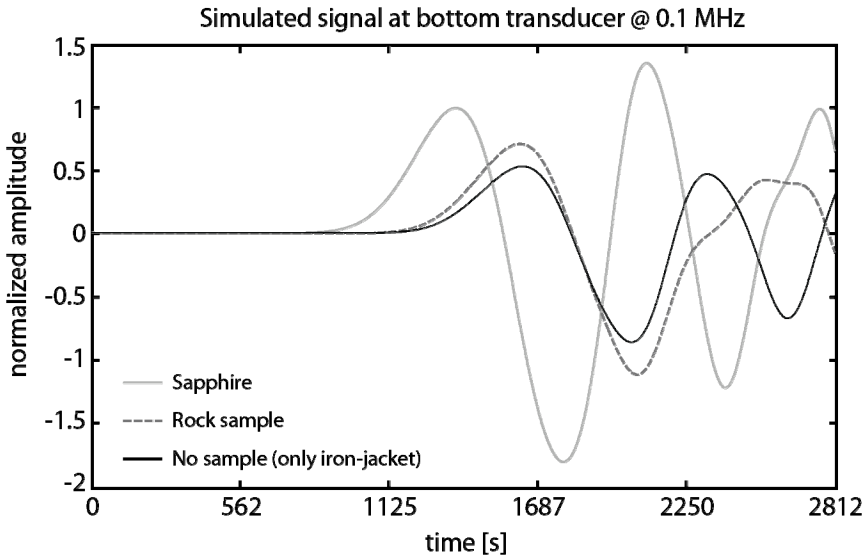**Simulated signal at bottom transducer @ 0.1 MHz**

Fig. 6. Simulated vertical displacement at bottom transducer for the setup shown in Fig. 5. The reference signal (gray line) using a sapphire sample arrives first. The time delay of the signal for the rock sample (dashed line) is normally used to estimate the velocity of the rock. However, the signal with no sample (black line; wave propagation through the iron jacket only) may disturb the signal for the rock.

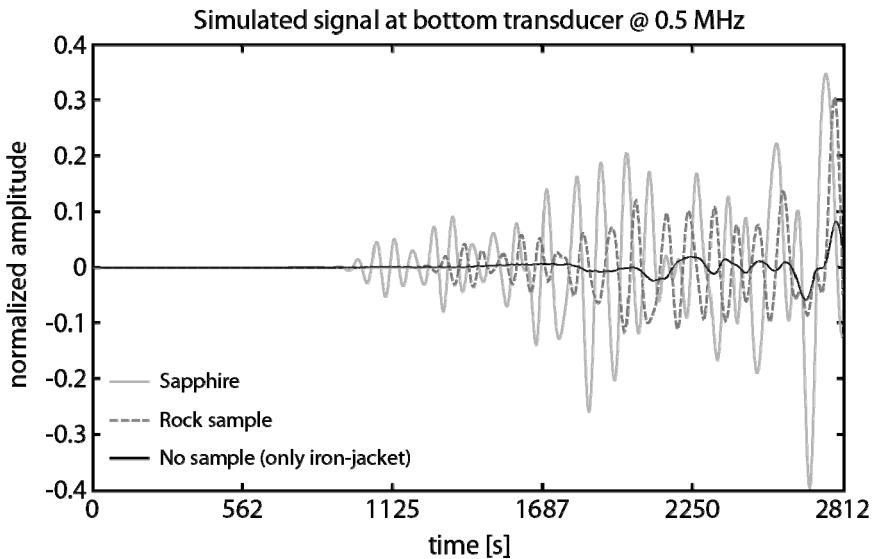**Simulated signal at bottom transducer @ 0.5 MHz**

Fig. 7. Same as Fig. 6 but using a source with a fundamental frequency of 0.5 MHz. The influence of the iron jacket is not as strong as for the lower frequency.

It appears that the wave velocity is higher at low frequencies. However, this observation is due to the fact that part of the energy propagates through the thin metal cover sleeve (jacket), which influences the measured signal at the bottom receiver. This effect is more dominant for waves propagating at 0.1 MHz (black line in Fig. 6 *versus* black line in Fig. 7).

Based on first-arrival time picking in the numerical simulations, our best estimate for the velocity of the rock is 5033 m/s at 0.5 MHz (Fig. 7), instead of 5100 m/s, which is the correct value we assigned to the rock sample. This too low value would also be estimated in the real experiment.

These observations are important to interpret standard ultrasonic velocity measurements usually performed in the laboratory. Specific numerical experiments, like the ones presented here, are necessary to optimize the velocity determination. The influence of an iron jacket (sometimes required for specific issues) has to be taken into account.

5. CONCLUSIONS

We presented two numerical studies, which support laboratory investigations. The experimental design can be optimized based on the results of the computer experiments. Simulation of seismic wave propagation on the laboratory scale (somewhere between micro- and field-scale) can help understand and correct findings of real experiments.

For attenuation measurements we suggest an optimized positioning of the sensors if possible. A cut-off frequency has to be determined, above which unwanted resonance effects disturb the results. This cut-off frequency also depends on the elastic properties of the considered sample.

For ultrasonic velocity measurements we suggest to take into account the effects of the used jacket and the pieces between the sample and the transducers. All of these experimental pieces have a strong frequency-dependent effect on the recorded signals. Only specific numerical investigations will allow taking them into account.

References

Batzle, M., D. Han, and R. Hofmann (2006), Fluid mobility and frequency-dependent seismic velocity – Direct measurements, *Geophysics* **71**, 1, N1-N9, DOI: 10.1190/1.2159053.

Burlini, L., L. Arbaret, G. Zeilinger, and J.-P. Burg (2005), High-temperature and pressure seismic properties of a lower crustal prograde shear zone from the Kohistan arc, Pakistan, *Geol. Soc. London Spec. Publ*. **245**, 187-202, DOI: 10.1144/GSL.SP.2005.245.01.09.

Burlini, L., S. Vinciguerra, G. Di Toro, G. De Natale, P. Meredith, J.-P. Burg (2007), Seismicity preceding volcanic eruptions: New experimental insights, *Geology* **35**, 2, 183-186, DOI: 10.1130/G23195A.1.

Caricchi, L., L. Burlini, and P. Ulmer (2008), Propagation of P- and S-waves in magmas with different crystal contents: Insights into the crystallinity of magmatic reservoirs, *J. Volcanol. Geoth. Res*. **178**, 4, 740-750, DOI: 10.1016/j.jvolgeores.2008.09.006.

Christensen, N.I. (1979), Compressional wave velocities in rocks at high temperatures and pressures, critical thermal gradients, and crustal low-velocity zones, *J. Geophys. Res*. **84**, B12, 6849-6857, DOI: 10.1029/JB084iB12 p06849.

Ferri, F., L. Burlini, B. Cesare, and R. Sassi (2007), Seismic properties of lower crustal xenoliths from El Hoyazo (SE Spain): Experimental evidence up to partial melting, *Earth Planet. Sc. Lett.* **253**, 1-2, 239-253, DOI: 10.1016/j.epsl.2006.10.027.

Jackson, I., and M.S. Paterson (1987), Shear modulus and internal friction of calcite rocks at seismic frequencies: pressure, frequency and grain size dependence, *Phys Earth Planet. In*. **45**, 4, 349-367, DOI: 10.1016/0031-9201(87) 90042-2.

Kern, H., S. Gao, Z. Jin, T. Popp, and S. Jin (1999), Petrophysical studies on rocks from the Dabie ultrahigh-pressure (UHP) metamorphic belt, central China: implications for the composition and delamination of the lower crust, *Tectonophysics* **301**, 3-4, 191-215, DOI: 10.1016/S0040-1951(98)00268-6.

Kono, Y., M. Ishikawa, and M. Arima (2004), Discontinuous change in temperature derivative of Vp in lower crustal rocks, *Geophys. Res. Lett*. **31**, 22, L22601, DOI: 10.1029/2004GL020964.

Lakes, R.S. (2009), *Viscoelastic Materials*, Cambridge University Press, New York, 461 pp.

Madonna, C., and N. Tisato (2013), A new Seismic Wave Attenuation Module to experimentally measure low-frequency attenuation in extensional mode, *Geophys. Prospect*. **61**, 2, 302-314, DOI: 10.1111/1365-2478.12015.

O'Connell, R.J., and B. Budiansky (1977), Viscoelastic properties of fluid-saturated cracked solids, *J. Geophys. Res*. **82**, 36, 5719-5735, DOI: 10.1029/JB082 i036p05719.

Saenger, E.H., N. Gold, and S.A. Shapiro (2000), Modeling the propagation of elastic waves using a modified finite-difference grid, *Wave Motion* **31**, 1, 77-92, DOI: 10.1016/S0165-2125(99)00023-2.

Saenger, E.H., S.A. Shapiro, and Y. Keehm (2005), Seismic effects of viscous Biot-coupling: finite difference simulations on micro-scale, *Geophys. Res. Lett.* **32**, 14, L14310, DOI: 10.1029/2005GL023222.

Saenger, E.H., F. Enzmann, Y. Keehm, and H. Steeb (2011), Digital rock physics: Effect of fluid viscosity on effective elastic properties, *J. Appl. Geophys.* **74**, 4, 236-241, DOI: 10.1016/j.jappgeo.2011.06.001.

Spencer Jr., J.W. (1981), Stress relaxations at low frequencies in fluid saturated rocks: Attenuation and modulus dispersion, *J. Geophys. Res.* **86**, B3, 1803-1812, DOI: 10.1029/JB086iB03p01803.

Steiner, B., and E.H. Saenger (2012), Comparison of 2D and 3D time-reverse imaging – A numerical case study, *Comput. Geosci.* **46**, 174-182, DOI: 10.1016/j.cageo.2011.12.005.